IEEE Access
Multidisciplinary | Rapid Review | Open Access Journal

Received 5 December 2023, accepted 4 January 2024, date of publication 10 January 2024,
date of current version 18 January 2024.

Digital Object Identifier 10.1109/ACCESS.2024.3352256

APPLIED RESEARCH

Compact Muti-Frequency Band-Pass Filters Based on High-Order Mode of Folded Line Spoof Surface Plasmon Polaritons Waveguide

SIYU YANG[1], SHUANG LIU[1,2], FACHUN HE[1], HUALI ZHU[2], LIANGJING WANG[1], DAN LEI[1], CHAN GAO[1], JUN YAN[3], AND SHUANG LIU[1]

[1]School of Mathematics and Science, Chengdu University of Technology, Chengdu 610000, China
[2]School of Electronic Science and Engineering, University of Electronic Science and Technology of China, Chengdu 610000, China
[3]China Electronics Technology Group Corporation 10th Research Institute, Chengdu 610000, China

Corresponding author: Shuang Liu (ranranshuangshuang@163.com)

This work was supported in part by the Chengdu University of Technology 2021 Young and Middle-Aged Backbone Teachers Development Funding Program under Grant 10912-JXGG2021-06751; in part by the Chengdu University of Technology 2022 Young and Middle-Aged Backbone Teachers Development Funding Program under Grant 10912-JXGG2022-01782; in part by the Second Batch of the Ministry of Education Industry-University Cooperative Education Project, in 2022, under Grant 220903117301555; in part by the Sichuan Provincial Natural Science Foundation of China under Grant 23NSFSC4751; in part by the Natural Science Foundation of Sichuan Province under Grant 2022NSFSC0332; and in part by the Chengdu University of Technology 2023 Young and Middle-Aged Backbone Teachers Development Funding Program under Grant 10912-JXGG2023-09014.

ABSTRACT We proposed a folded line spoof surface plasmonic polaritons (SSPPs) waveguide that allows for efficient and strongly constrained microwave SSPPs transmission. The dispersion characteristics of SSPPs waveguides based on folded line unit is investigated. Compared to conventional rectangular-grooved SSPPs waveguide with the same cut-off frequency, the lateral dimension of the folded line SSPPs waveguide can be reduced to 56%. The results show that the folded line SSPPs waveguide has stronger field binding as well as better miniaturization advantages. In order to validate the proposed design, a dual-band band-pass filter is designed based on the high-order mode of the proposed unit and we then add an asymmetric structure to achieve a tri-band band-pass filter with good performance. In addition, a band-pass filter with wide stopband between two pass bands is designed by incorporating an interdigital finger in the folded line unit, whose width of the stopband can be increased by 50% compared to the filter without interdigital finger. By optimizing the length of interdigital finger, two notch bands are respectively obtained in two pass bands of a dual-band pass-band filter. At the same time, the stopband is also widened. Four proposed filters are fabricated and the measurement results are in good agreement with the simulated ones, verifying the feasibility of the structure. The proposed SSPPs structure can significantly enhance the flexibility and universality of the filter. Additionally, these filters offer compact structures, wide stopbands, and hold immense potential for application in integrated devices.

INDEX TERMS Band-pass filter, folded line, notch band, spoof surface plasmonic polaritons (SSPPs).

I. INTRODUCTION

Surface plasmonic polaritons (SPPs) is a metal-specific electromagnetic phenomenon, when light or electromagnetic waves incident on the interface between the metal and the medium, the free electrons in the metal conductor undergo a collective oscillation, resulting in a surface electromagnetic mode [1]. SPPs modes have stronger surface confinement to electromagnetic fields. However, metals are equivalent to ideal conductors in lower frequency bands such as terahertz and microwave, where SPPs does not exist [2]. In order to obtain the field-binding and field-enhancing effects of surface

The associate editor coordinating the review of this manuscript and approving it for publication was Zhaojun Steven Li.

plasmonic polaritons in the low-frequency band. In 2004, Pendry, et al. proposed that the concept of spoof surface plasmon polaritons (SSPPs) to mimic the characteristics of SPPs in the optical region [3]. Effective matching leaps for spoof surface plasmonic polaritons have been proposed to solve the compatibility problem of planar circuits and systems [4], [5]. For SSPPs, the dispersion characteristics are artificially controlled by adjusting the cell size of the slots and are widely used in design studies [6], [7], [8], [9], [10]. Spoof surface plasmon polaritons are widely employed for various functional devices at microwave and terahertz frequencies, such as many filters [11], [12], [13], [14], antennas [15], [16], power dividers [17], [18], [19], etc.

With the rapid development of SSPPs, it is of great significance to study compact SSPPs transmission line [21], [22]. References [23], [24], and [25] report that some band-pass filters have achieved some degree of miniaturization by optimizing the lateral equivalent dimensions. Wide stopband has the potential for lower crosstalk, so it is important to investigate increasing the stopband width. However, the improvement of this problem is rarely mentioned in the stopband filters [26], [27]. Multi-band notch filters are indispensable devices in multi-band communication systems, which can simultaneously suppress multiple unwanted spectra. But, band-pass filters with notch band are mostly obtained by adding defected ground or loading complex resonators [28], [29], [30], [31], [32]. The tri-band filter in [33] combines the multi-mode resonance and cut-off characteristics of SSPPs to contribute to a tri-band band-pass response. Therefore, the research on compact SSPPs multi-mode filters with wide stopbands and flexible design of notch band positions in the pass band is highly significant for enhancing the overall system performance.

In this paper, we propose a novel folded line spoof surface plasmonic polaritons (SSPPs) waveguide that allows for efficient and strongly constrained microwave SSPPs transmission. The dispersion characteristics of SSPPs waveguides based on folded line units are investigated. The lateral dimension of the proposed SSPPs waveguide is reduced to 56% compared to a conventional rectangular SSPPs waveguide with the same cut-off frequency. Based on the high-order mode of SSPPs unit, a dual-band band-pass filter with higher transmission coefficients and lower reflection coefficients has been designed. By adding asymmetric structure to the dual-band band-pass filter, a tri-band band-pass filter with good performance has also been designed, which also has the advantages of miniaturization. In addition, by loading interdigital fingers on the dual-band band-pass filter, the width of the stopband can be increased by 50% in the frequency range of 8 GHz to 9.6 GHz. By optimizing the length of interdigital finger, two notch bands appear at the frequencies of 6.7 GHz-7.8 GHz and 14.3 GHz-15.1 GHz, respectively. Additionally, the stopband is also widened. In order to verify the performance, four filters based on the proposed folded line SSPPs structure were fabricated and measured. The measurement results are in good agreement with the simulated ones, verifying the feasibility of the structure. Compared with previous studies on work [20], [21], [22], [23], [24], [25], [28], [29], [30], [31], [32], [33], the proposed filters have the advantages of compact structure, wide stopband, and multiple unwanted spectra are suppressed by notch band.

II. BAND-PASS FILTERS BASED ON THE HIGH-ORDER MODE OF FOLDED LINE SSPPs WAVEGUIDE

A. DISPERSION CHARACTERISTIC OF SSPPS UNIT

The proposed SSPPs waveguide consists of a periodic array of folded line units. The schematic diagrams of the folded line unit and the conventional rectangular-grooved structure are shown in Fig. 1(a). The depth of the folded line groove $h =$ 6.4 mm, depth of the conventional rectangular groove $h_t =$ 6.4 mm, length $w = 4$ mm, width $g = 0.2$ mm, line width $w_1 = 2$ mm, as well as the period $d = 6$ mm. Yellow and blue colors indicate the metal layer and dielectric substrate of the cell. The dielectric substrate is a 0.508 mm Rogers 5880 with a dielectric constant (ε_r) of 2.2 and the loss angle tangent of 0.0009. And the SSPPs unit is backed by a metal ground. It can affect the propagation characteristics of SSPPs, causing the electromagnetic field of SSPPs to be more tightly confined near the metal surface and reducing the losses propagating into the medium.

To investigate the properties of the proposed SSPPs waveguide, we analyze the high-order mode dispersion characteristics and electric field distribution of the folded line SSPPs cell. High-order mode appear when the equivalent groove depth is greater than the period [34], [35]. Fig. 1(b) shows the dispersion diagram of the folded line unit. The results show that the dispersion curves of all three modes of SSPPs are located in the right side of the light, which reflects the typical slow-wave nature of the structure. The dispersion curves start from intersecting the dispersion curve of light in free space, and gradually deviate from the light as the intrinsic phase shift value increases until it reaches the maximum frequency value, i.e., which is the cut-off frequency. As the dispersion curve approaches the cut-off frequency, the binding capacity of the field to the SSPPs reaches its maximum strength. As shown in Fig. 1(a) and Fig. 1(b), while the period $d = 6$ mm and the groove depth $h = h_t = 6.4$ mm, the cut-off frequencies of Mode 0, Mode 1 and Mode 2 of the proposed folded line structure are respectively 3.1 GHz, 8.6 GHz and 15.3 GHz, and the cut-off frequencies of Mode 0 and Mode 1 of the conventional structure are 7.4 GHz and 17.6 GHz, respectively. This indicates that the folded cell has advantages in frequency response range and strong field confinement. The cut-off frequency of the Mode 0 of both the folded line structure and the conventional structure is 3.1 GHz when the period is constant, $h = 6.4$ mm and $h_t = 17$ mm. The lateral dimension of the folded line SSPPs cell can be reduced to 56% of the conventional structure. Therefore, it has great field confinement capability and size advantage.

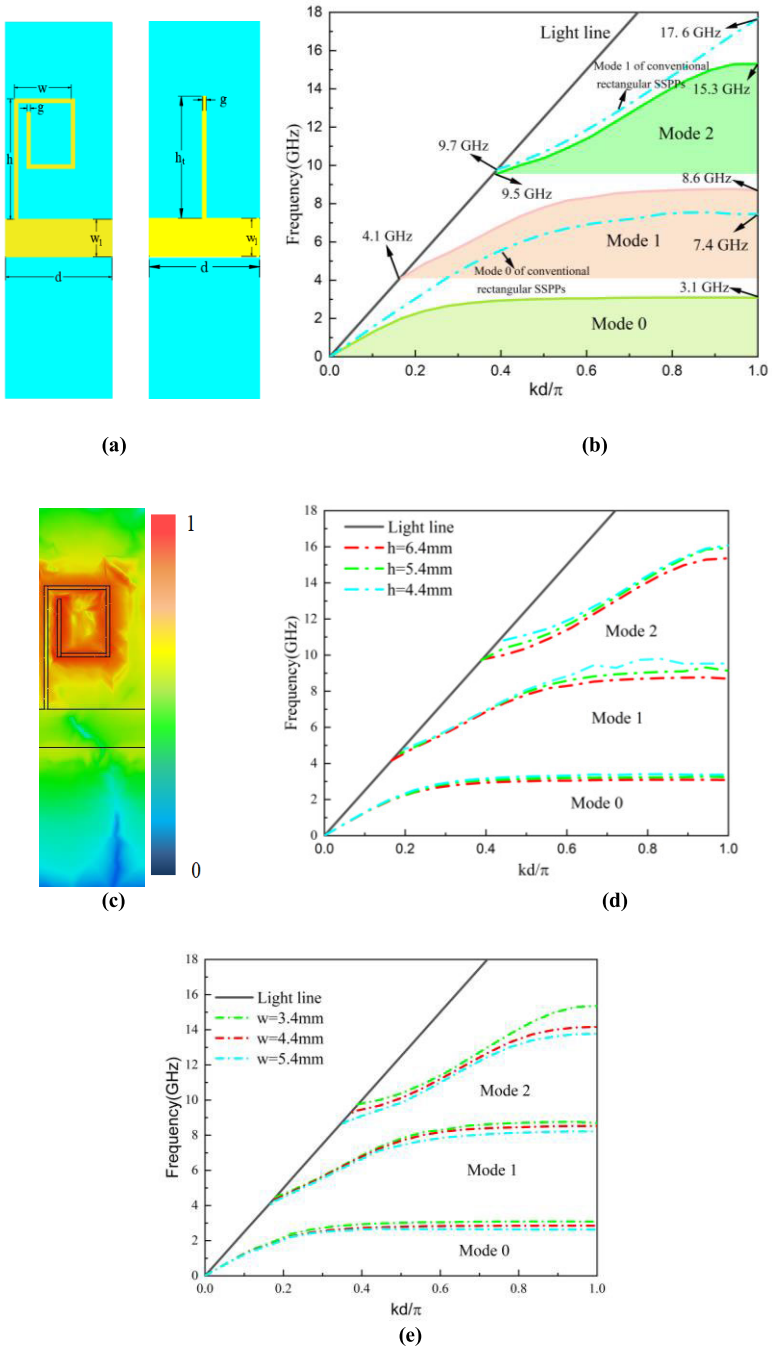

FIGURE 1. (a) Conventional rectangular-groove SSPPs unit and folded line SSPPs unit. (b) Dispersion characteristics of the folded line SSPPs unit and conventional grooves SSPPs unit. (c) The simulated electric field distribution. (d) Dispersion characteristics of SSPPs unit with different *h*. (e) Dispersion characteristics of SSPPs unit with different *w*.

Fig. 1(c) shows the simulated electric field distribution of the folded line unit. The results show that the electric field is mainly concentrated in the groove part of the folded line unit, which demonstrating great field confinement. From (d)-(e), it can be obtained that the cut-off frequencies of its fundamental and high-order mode gradually decrease with the increase of the groove depth h and the groove length w. Therefore, the cut-off frequency of the folded line SSPPs can be independently determined by w and h, which provides great design flexibility.

B. DUAL-BAND BAND-PASS FILTER REALIZATION

As shown in Fig. 1(b), there is no overlapping part between the fundamental and high-order modes. This shows that the single mode propagation is available and it is feasible to

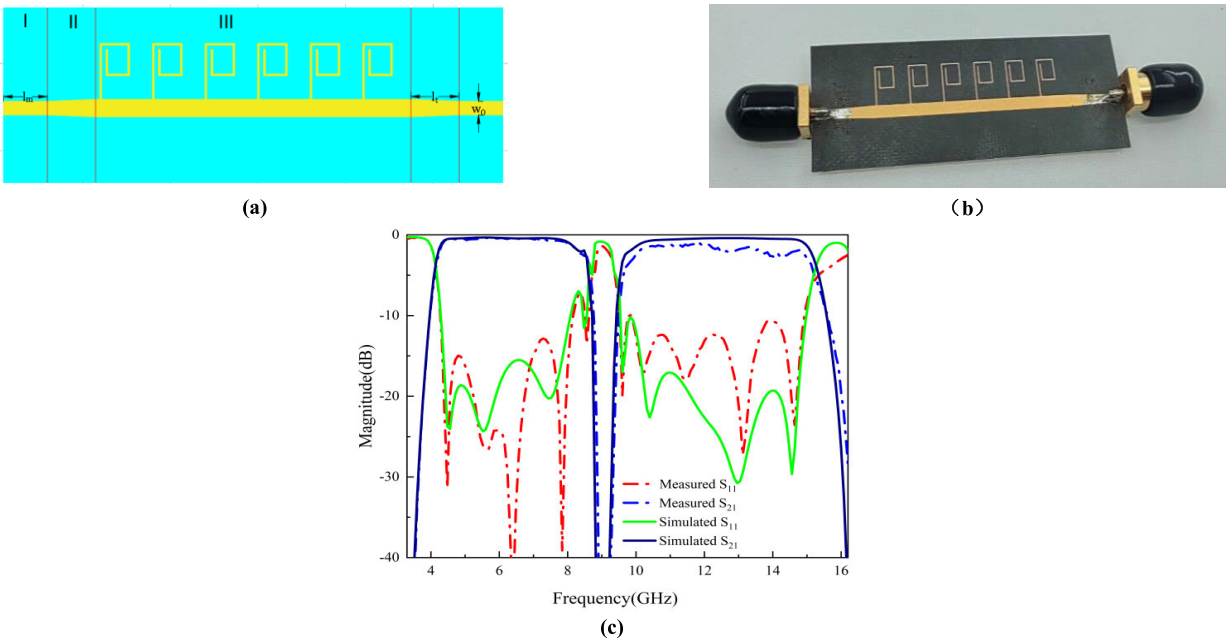

FIGURE 2. (a) Schematic configuration of the structure of the dual-band filter. (b) Photograph of the proposed dual-band filter. (c) Comparison of simulated and measured S-parameters of the dual-band filter.

use the high-order mode for the design of band-pass filter. Therefore, a dual-band band-pass filter was constructed based on the mode 1 and mode 2 of the SSPPs cell, as shown in Fig. 2(a). It consists of three regions. In Region I, the width of the microstrip line $w_0 = 1.55$ mm to achieve 50-ohm to match the SMA connector and the length $l_m = 5\ mm$. Region II is a simple trapezoidal transition, which connects the microstrip line to the proposed SSPPs structure. Region III is an SSPPs structure consisting of six identical unit structures with the same parameters as those in Fig. 1(a).

Characteristic impedance properties of mode 0-2 of the folded line SSPPs waveguide are investigated using the method proposed in [36]. Based on the method of extracting the characteristic impedance given in [36], the characteristic impedance of the proposed SSPP waveguide is 35 ohm, 40 ohm, and 38 ohm at 2 GHz, 6.5 GHz, and 14.5 GHz, respectively. For the microstrip excitation strategy, microstrips with a length of 10.5 mm and widths of 2.6 mm, 2.3 mm, and 2.1 mm are connected to both ends of the SSPPs waveguide. The simulated S-parameters are shown in Fig. 3(a)-(c), where reflection (S_{11}) lower than -30 dB is observed at 2 GHz, 6.5 GHz, and 14.5 GHz, respectively. It can be obtained the characteristic impedance of mode 1-2 of the proposed SSPPs waveguide are similar, therefore the impedance matching between the microstrip line and the SSPPs array can be achieved by optimizing the length l_t of the trapezoid-structure in the region II. The optimized length l_t is 5.5 mm. And this whole dual-band band-pass filter structure is backed by the metal ground, which is intended to enhance the field binding.

Based on the above structure, the S-parameters of the proposed SSPPs filter is simulated, which are shown in Fig. 2(c). From Fig. 2(c), the first passband is from 4.1 GHz to 8.6 GHz and the second passband is from 9.5 GHz to 15.3 GHz. It is obvious that, the two passbands of the proposed filter correspond well to the first high-order mode and the second high-order mode of the SSPPs unit, respectively. The dual-band filter is fabricated based on the Rogers 5880 with the thickness of 0.508mm. Fig. 2(b) shows the photograph of the proposed filter. The proposed filter is measured using the VNA and the measurement results are also shown in Fig. 2(c). As shown in Fig.2(c), the measured insertion loss is lower than 1 dB and the average return loss is better than 15 dB within two pass bands, which are consistent with the simulation results. Some small deviations are mainly caused by fabrication tolerances.

In order to further reveal the working principle of the high-order mode filter based on the folded line SSPPs structure, the simulated electric field distribution of the filter is investigated. As shown in Fig. 4(a)-(c), the 5 GHz and 11 GHz microwaves located in the pass band can be efficiently transmitted through the entire band-pass filter with small losses. The 9 GHz microwave, which is placed in the out of passband, terminates in the first SSPPs cell.

III. APPLICATION OF FOLDED LINE SSPPs WAVEGUIDE IN THE MINIATURIZED MULTI-BAND FILTER DESIGN

A. TRI-BAN BAND-PASS FILTER

Based on the high-order mode SSPPs cell above, a tri-band band-pass filter is designed by incorporating an asymmetric fold line structure as shown in Fig. 5(a). The filter consists of six identical asymmetric fold line SSPPs cells. The dimensional parameters of the asymmetric folded line cell are: $w = 4\ mm$, $h_1 = 2$ mm, $h_2 = 1.7$ mm, $g = 0.2$ mm. The dispersion curves of the SSPPs unit are shown

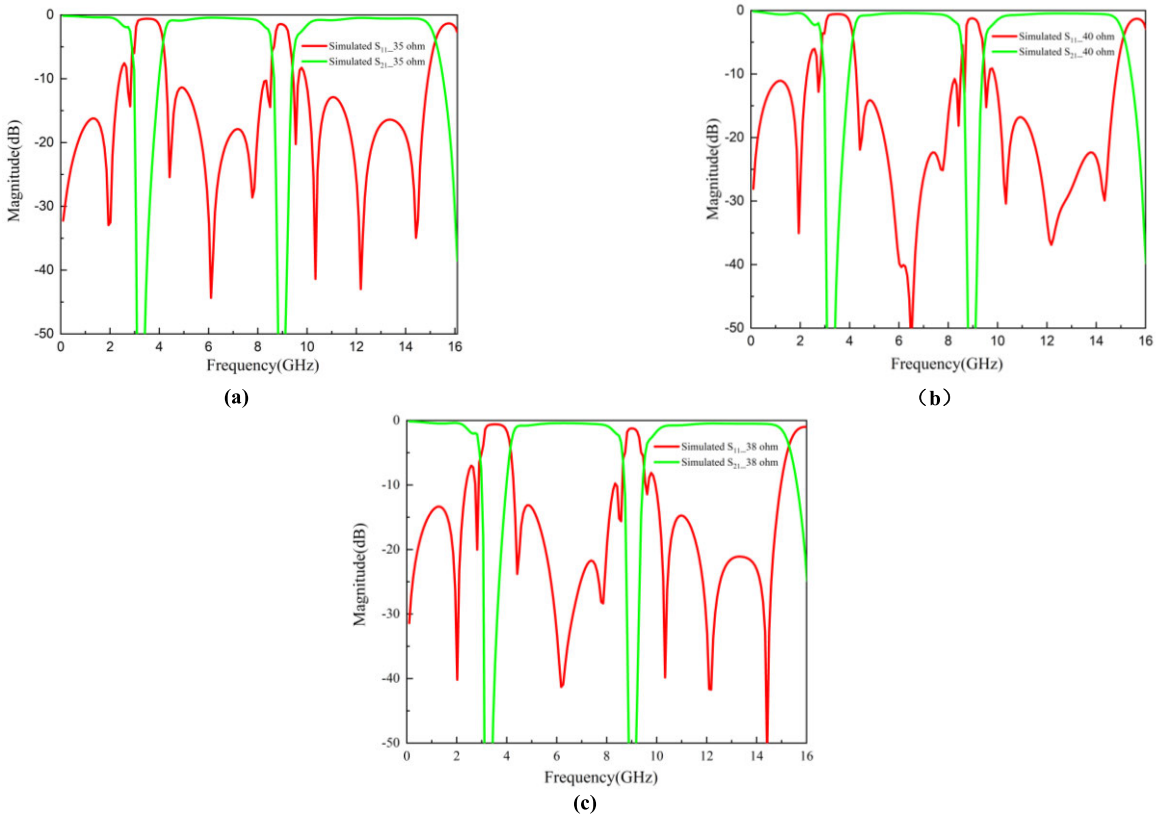

FIGURE 3. Simulated impedance matching of folded line band-pass filter with a microstrip of (a)35 Ω, (b)40 Ω, and (c)38 Ω, corresponding to matching at 2 GHz, 6.5 GHz, and 14.5 GHz, respectively.

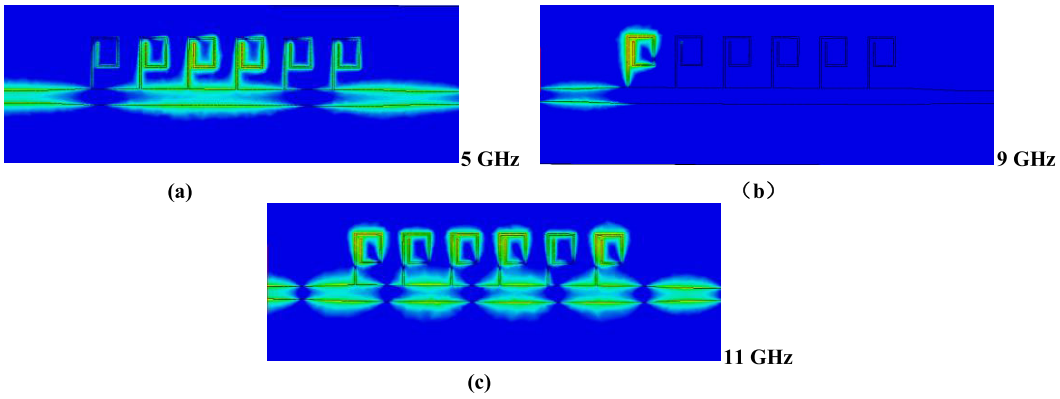

FIGURE 4. Electric field distributions at (a)5 GHz, (b)9 GHz and (c)11 GHz, respectively.

in Fig. 5(b), where three high-order modes appear. Compared with rectangular-grooved SSPPs waveguide, the lateral dimension of SSPPs waveguide incorporating an asymmetric structure can be reduced to 46%. It still has the characteristics of miniaturization. The tri-band filter is fabricated based on the Rogers 5880 with the thickness of 0.508mm. Photograph of the tri-band band-pass filter with SMA connectors are displayed in Fig. 5(c).

Fig. 5(d) shows the simulated and measured S-parameter of the tri-band band-pass filter. Its measurements and simulations are almost identical in the first and second passbands, with a small deviation in the third passband, probably due to energy loss at higher frequencies during the measurements. As shown Fig. 5(d), the measured S_{21} in three passbands are all less than 0.7dB and the measured average return loss is better than 15 dB. It can also be seen that the two narrow and deep stopbands are obtained among three passbands. Two stopbands are from 5.4 GHz to 6.9 GHz and 8.8 GHz to 9.6 GHz, which coincides with the dispersion curve of high-order mode folded line cell.

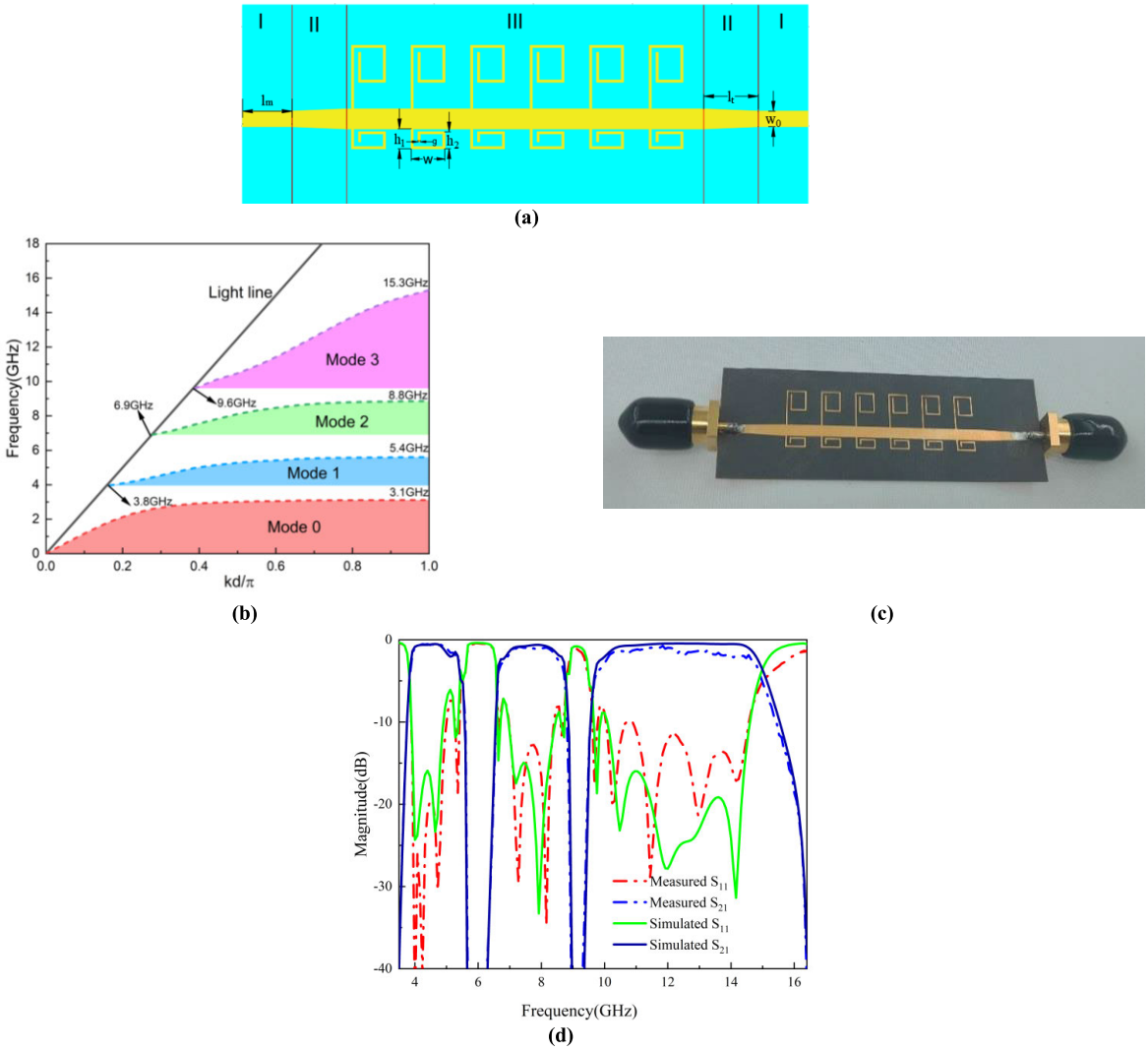

FIGURE 5. (a) Schematic configuration of the structure of the tri-band band-pass filter. (b) Dispersion characteristics of the SSPPs cell used in the tri-band filter. (c) Photograph of the proposed tri-band band-pass filter. (d) Comparison of simulated and measured S-parameters of the tri-band filter.

B. MULTI-FREQUENCY BAND-PASS FILTER WITH INTERDIGITAL FINGER

In order to broaden the stopband and enhance isolation between passbands, we loaded an interdigital finger structure in the folded line cell of the dual-band filter based on SSPPs designed above. The folded line SSPPs cell with interdigital finger is shown in Fig. 6(a). The SSPPs cell is also backed by a metal ground, which is intended to enhance the field binding. Fig. 6(b) shows the equivalent circuit model of the interdigital finger structure. The interdigital finger structure enables the enhancement of the effective capacitance with lower loss and resonant frequency compared to split ring resonators (SRRs) and complementary SRRs of the same size [37].

By adjusting the length of interdigital finger, the value of the total capacitance can be changed, which in turn affects the resonant frequency. Setting the appropriate structural size can regulate the notch position, which provides a solid foundation for the design of notch filters and also favorably support the design of muti-band band-pass filters with wider stopband.

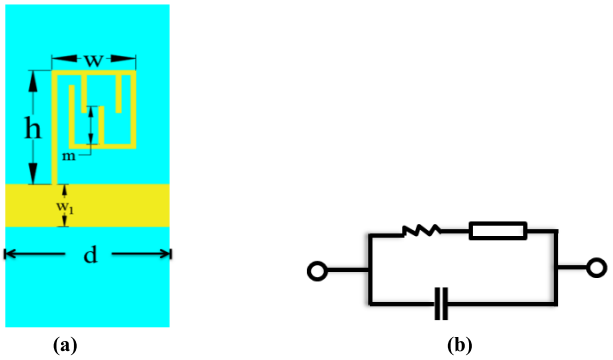

FIGURE 6. (a) Schematic of the folded line unit with interdigital finger. (b) Equivalent circuit model.

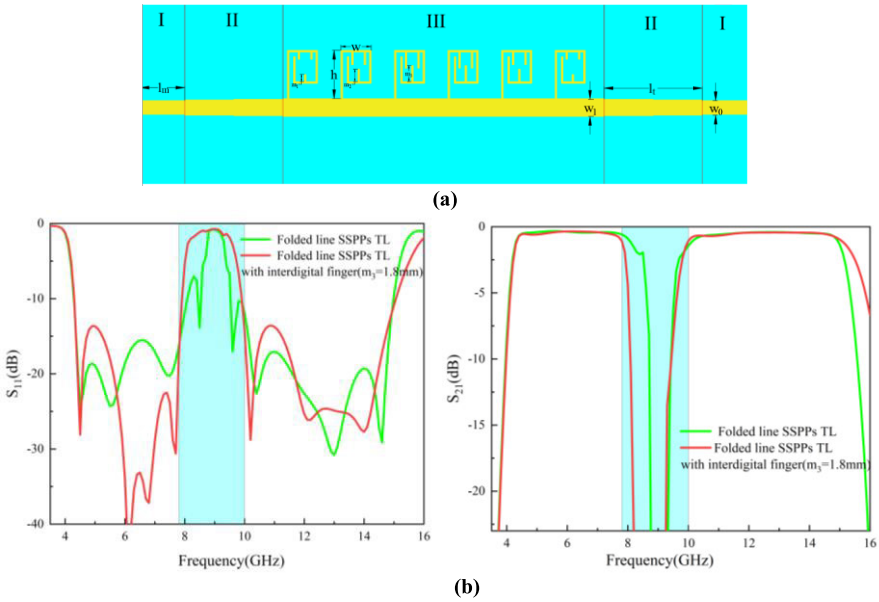

FIGURE 7. (a) Schematic configuration of band-pass filter with interdigital finger ($m_3 = 1.8$ mm). (b) Comparison of simulated S-parameters between band-pass filter with interdigital finger ($m_3 = 1.8$ mm) and band-pass filter without interdigital finger.

Based on the above analysis, a dual-band band-pass filter based on the folded line cell with interdigital finger is designed, which is shown in Fig. 7(a). Detailed dimensions are shown in Table 1. The period d and the width g remain unchanged, $d = 6$ mm and $g = 0.2$ mm, respectively. The length of interdigital finger labeled m_1-m_3 is gradually increased from 0.8 mm to 1.8 mm. And the whole filter is backed by a metal ground, which is intended to enhance the field binding. The proposed filter consists of three regions. Similar to the design of the previous dual-band filter, a 50-ohm microstrip line with a width w_0 of 1.55 mm is set in Region I to match the SMA connector and Region II is a simple trapezoidal transition, which connects the microstrip line to the proposed SSPPs structure. Region III is the SSPPs structure consisting of six folded line cells with interdigital finger.

The simulated S_{11} and S_{21} of the proposed SSPPs filter with interdigital finger are shown in Fig. 7(b), which is compared with the dual-band filter without interdigital finger that is designed above. The passband of the proposed filter is consistent with the dual-band band-pass without interdigital finger, and its lateral dimension is only 84% of the dual-band band-pass filter unit structure. As shown in Fig. 7(b), the stopband of the proposed filter with interdigital finger is from 8 GHz to 9.6 GHz. Compared to the dual-band filter without the interdigital finger, the stopband of the proposed filter with interdigital finger is increased by 50%. As a result, the band-pass filter with interdigital finger has a stronger rejection capability in the stopband range, thus providing better filtering. This is especially important in applications such as reducing interference or preventing signal leakage.

The proposed filter is fabricated based on the Rogers 5880 with the thickness of 0.508mm and the photograph is shown in Fig. 8(a). The measured results, as shown in Fig. 8(b), agree well with the simulated results. The measured insertion loss is less than 0.5 dB and the average return loss is better than 18 dB in the frequency band from 4.1 GHz to 8 GHz. The measured insertion loss is less than 1.5 dB and the average return loss is better than 15 dB in the frequency band from 9.6 GHz to 15.3 GHz.

TABLE 1. Design parameters of dual-band band-pass filter with the interdigital finger (unit: mm).

l_m	w_0	l_t	w_1	m_1	m_2	m_3	h	w
5	1.55	11	2	0.8	1.4	1.8	5.4	3.4

In summary, the designed filter not only has the advantage of miniaturization, but also broadens the stopband bandwidth between passbands and ensures good performance.

Based on the analysis of interdigital finger structure shown in Fig. 6, the notch position can be regulated by adjusting the dimensions of the interdigital finger. Without changing other dimensions of the proposed dual-band filter with interdigital finger folded line cell designed in Fig. 7, the length of the interdigital finger m_3 is set to 3mm, resulting in two notch bands appearing in the respective passbands. As shown in Fig. 9(a), in the blue region the stopband of band-pass filter with the interdigital finger still yields a slightly wider stopband than the dual-band filter without the interdigital finger designed in section II. In the case of the widened stopband, two notch bands appear at 6.7 GHz−7.8 GHz and 14.3 GHz−15.1 GHz, respectively. The simulated and measured results are shown in Fig. 9(b) and the photograph of the fabricated filter is shown in Fig. 9(c). The measured results are in agreement with the simulated ones, which indicates that the designed filter has the advantages of miniaturization, wide stopband, and has the notch band in the passband. And

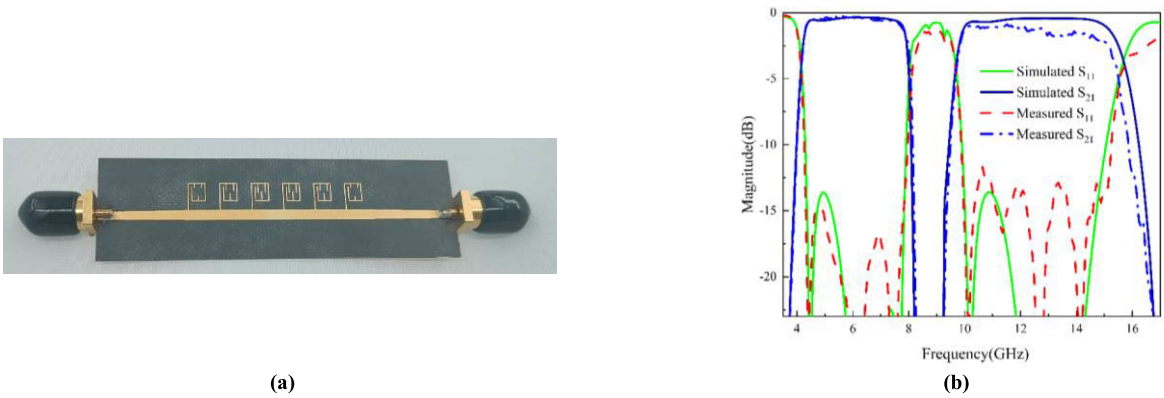

FIGURE 8. (a) Photograph of the proposed band-pass filter with interdigital finger ($m_3 = 1.8$ mm). (b) Comparison of simulated and measured S-parameters of band-pass filter with interdigital finger ($m_3 = 1.8$ mm).

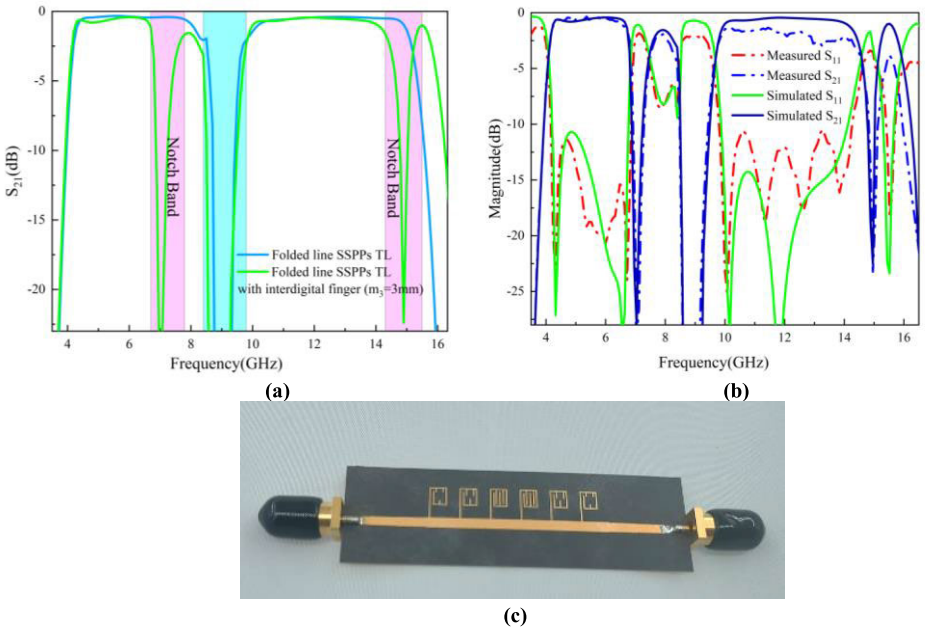

FIGURE 9. (a) Comparison of simulated S_{21} of the band-pass filter with interdigital finger ($m_3 = 3$ mm) and the band-pass filter without interdigital finger. (b) Comparison of simulated and measured S-parameters of the proposed notch band-pass filter with interdigital finger ($m_3 = 3$ mm). (c) Photograph of the proposed notch band-pass filter with interdigital finger.

there are better advantages in improving the performance of the system, minimizing the interference, and achieving the desired frequency control.

In summary, by adjusting the size of the folded line structure with interdigital finger, the stopband bandwidth can be increased, which reduces interference between signals. Additionally, the notch position can be flexibly set within the frequency band to suppress unwanted signals.

IV. PERFORMANCE COMPARISON

Table 2 compares the performance of the proposed folded line band-pass filter with previously reported work. References [20], [21], and [22] report SSPPs transmission lines with strong field confinement. References [23], [24], and [25] reports some filter with only one passband based on high-order mode. However, our designed filters are based on multiple high-order modes, which can achieve multiple transmission passbands with strong field enhancement effect. The performance of notch band, widened stopband width, and enhanced channel crosstalk is achieved by adjusting the interdigital finger structure of SSPPs units. Although the filter in [28] has a notch band and four transmission passbands, it has no size advantage over the structure in this paper. The filters in [29], [30], [31], [32], and [33] have successfully realized 2-3 transmission passbands by adding defected ground or inserting the structure between the grooves of SSPPs transmission line grooves, or using muti-mode resonant SSPPs cell. The proposed filters in this paper can realize

TABLE 2. Comparison of the proposed band-pass filters with the previous design.

Ref.	Used modes	Number of notch bands	Notch band width (GHz)	Number of stopbands	Stopband width (GHz)	f_0 (GHz)	Fractional Relative Bandwidth	IL (dB)	Horizontal dimension (λg)
[20]	Mode 0	\	\	\	\	189.5	32.2%	\	\
[21]	Mode 0	\	\	\	\	4	200%	\	\
[22]	Mode 0	\	\	\	\	15	26.7%	\	0.2
[23]	Mode 1	\	\	\	\	7.79	43.38%	1.46	0.39
[24]	Mode 1	\	\	\	\	8	50%	1.7	0.24
[25]	Mode 1	\	\	\	\	11.5	60%	2	0.59
[28]	Mode 1, Mode 2, Mode 3	1	0.75	2	1.25, 1.9	5.7, 9.1, 11.4, 15.3	63.16%, 7.69%, 21.49%, 9.48%	0.7, 0.6, 0.7, 0.6	0.26, 0.41, 0.52, 0.69
[29]	Mode 1	1	0.5	\	\	5.28, 7.41	35.04%, 19.16%	1.01	0.27, 0.37
[30]	Mode 1	1	0.13	\	\	7.25, 9.98	40.12%, 20.64%	\	0.36, 0.51
[31]	Mode 0	1	0.28	\	\	3.84, 8.33	95.83%, 56.9%	\	0.18, 0.39
[32]	Mode 1	1	0.95	\	\	13.7, 20.6	35.95%, 4.41%	1.7, 1.7	0.44, 0.67
[33]	Mode 0, Mode 1	\	\	2	0.8, \	2.9, 5.6, 11	45.8%, 17.8%, 6.4%	3, 3.1, 5.2	0.11, 0.21, 0.4
This work	Mode 1, Mode 2	\	\	1	0.9	6.35, 12.4	70.87%, 46.77%	0.5,1	0.17, 0.34
	Mode 1, Mode 2, Mode 3	\	\	2	1.5, 0.8	4.6, 7.85, 12.45	34.78%, 24.2%, 45.78%	0.5, 0.5, 0.7	0.16, 0.27, 0.43
	Mode 1, Mode 2	\	\	1	1.6	6.05, 12.45	64.46%, 45.78%	0.5, 1.5	0.15, 0.3
	Mode 1, Mode 2	2	1.1, 0.8	1	1.2	5.4, 8.1, 12, 15.2	48.15%, 7.41%, 39.17%, 0.66%	0.5, 2, 2, 3	0.13, 0.2, 0.3, 0.37

f_0 is the central frequency and IL is the insertion loss

2-4 transmission passbands with the advantage of miniaturization by using multiple high-order modes. And the notch band position and stopband width can be flexibly adjusted without the requirement of additional resonance structures using the proposed folded line SSPPs cell with an interdigital finger, which can also increase the transmission passbands. Therefore, this structure can greatly increase the flexibility as well as the universality of the filter design. This makes it possible to apply the folded line band-pass filter to circuits and systems at various microwave frequency bands.

V. CONCLUSION

In this paper, a new type of folded line spoof surface plasmon polaritons (SSPPs) waveguide is proposed. Its lateral dimension can be significantly reduced to 56% of a conventional rectangular SSPPs cell. The results show that the proposed SSPPs waveguide has good dimensional advantages. Based on this, dual-band band-pass filter is designed. As well as a tri-band band-pass filter with good performance is obtained by adding asymmetric structure on the basis of a dual-band band-pass filter. And the stopband of the dual-band band-pass filter is made wider by adding an interdigital finger. By adjusting the length of the interdigital finger, two notch bands were made to appear at frequencies of 6.7 GHz-−7.8 GHz and 14.3 GHz-−15.1 GHz, respectively. The measured results are generally in agreement with the simulation results. These results show that the proposed work has good potential for microwave miniaturization, broadening the stopband, and designing notch bands.

REFERENCES

[1] W. L. Barnes, A. Dereux, and T. W. Ebbesen, "Surface plasmon subwavelength optics," *Nature*, vol. 424, no. 6950, pp. 824–830, Aug. 2003, doi: 10.1038/nature01937.

[2] E. Ozbay, "Plasmonics: Merging photonics and electronics at nanoscale dimensions," *Science*, vol. 311, no. 5758, pp. 189–193, Jan. 2006, doi: 10.1126/science.1114849.

[3] J. B. Pendry, L. Martíin-Moreno, and F. J. Garcia-Vidal, "Mimicking surface plasmons with structured surfaces," *Science*, vol. 305, no. 5685, pp. 847–848, Aug. 2004, doi: 10.1126/science.1098999.

[4] X. Shen, T. J. Cui, D. Martin-Cano, and F. J. Garcia-Vidal, "Conformal surface plasmons propagating on ultrathin and flexible films," *Proc. Nat. Acad. Sci. USA*, vol. 110, no. 1, pp. 40–45, Jan. 2013, doi: 10.1073/pnas.1210417110.

[5] H. F. Ma, X. Shen, Q. Cheng, W. X. Jiang, and T. J. Cui, "Broadband and high-efficiency conversion from guided waves to spoof surface plasmon polaritons," *Laser Photon. Rev.*, vol. 8, no. 1, pp. 146–151, Jan. 2014, doi: 10.1002/lpor.201300118.

[6] L. Ye, Y. Chen, Z. Wang, C. Zhu, J. Zhuo, and Q. H. Liu, "Compact spoof surface plasmon polariton waveguides and notch filters based on meander-strip units," *IEEE Photon. Technol. Lett.*, vol. 33, no. 3, pp. 135–138, Feb. 2021, doi: 10.1109/LPT.2020.3046837.

[7] B. Mazdouri, M. M. Honari, and R. Mirzavand, "Miniaturized spoof SPPs filter based on multiple resonators or 5G applications," *Sci. Rep.*, vol. 11, no. 1, p. 22557, Nov. 2021, doi: 10.1038/s41598-021-01944-6.

[8] H. Ling, B. Zhang, M. Feng, P. Qian, Y. Wang, Q. Wang, Y. Zhang, and A. Song, "Multi frequency multi bit amplitude modulation of spoof surface plasmon polaritons by Schottky diode bridged interdigital SRRs," *Sci. Rep.*, vol. 11, no. 1, p. 19181, Sep. 2021, doi: 10.1038/s41598-021-98846-4.

[9] L. Li, L. Dong, P. Chen, and K. Yang, "Multi-band rejection filters based on spoof surface plasmon polaritons and folded split-ring resonators," *Int. J. Microw. Wireless Technol.*, vol. 11, no. 8, pp. 774–781, Oct. 2019, doi: 10.1017/S1759078719000369.

[10] Q. Le Zhang and C. H. Chan, "Spoof surface plasmon polariton filter with reconfigurable dual and non-linear notched characteristics," *IEEE Trans. Circuits Syst. II, Exp. Briefs*, vol. 68, no. 8, pp. 2815–2819, Aug. 2021, doi: 10.1109/TCSII.2021.3067936.

[11] Y. J. Guo, K. D. Xu, Y. Liu, and X. Tang, "Novel surface plasmon polariton waveguides with enhanced field confinement for microwave-frequency ultra-wideband bandpass filters," *IEEE Access*, vol. 6, pp. 10249–10256, 2018, doi: 10.1109/ACCESS.2018.2808335.

[12] L. Jidi, X. Cao, J. Gao, H. Yang, S. Li, and T. Li, "An ultra-thin and compact band-pass filter based on spoof surface plasmon polaritons," *IEEE Access*, vol. 8, pp. 171416–171422, 2020, doi: 10.1109/ACCESS.2020.3024596.

[13] H. Zhu, Y. Zhang, L. Ye, Y. Li, Y. Chen, R. Xu, and B. Yan, "Compact terahertz on-chip filter with broadband rejection based on spoof surface plasmon polaritons," *IEEE Electron Device Lett.*, vol. 43, no. 6, pp. 970–973, Jun. 2022, doi: 10.1109/LED.2022.3171292.

[14] Y.-J. Guo, K.-D. Xu, X. Deng, X. Cheng, and Q. Chen, "Millimeter-wave on-chip bandpass filter based on spoof surface plasmon polaritons," *IEEE Electron Device Lett.*, vol. 41, no. 8, pp. 1165–1168, Aug. 2020, doi: 10.1109/LED.2020.3003804.

[15] K. Zhuang, J. Geng, K. Wang, H. Zhou, Y. Liang, X. Liang, W. Zhu, R. Jin, and W. Ma, "Pattern reconfigurable antenna applying spoof surface plasmon polaritons for wide angle beam steering," *IEEE Access*, vol. 7, pp. 15444–15451, 2019, doi: 10.1109/ACCESS.2019.2895106.

[16] X.-F. Zhang, J. Fan, and J.-X. Chen, "High gain and high-efficiency millimeter-wave antenna based on spoof surface plasmon polaritons," *IEEE Trans. Antennas Propag.*, vol. 67, no. 1, pp. 687–691, Jan. 2019, doi: 10.1109/TAP.2018.2879847.

[17] J. Wang, L. Zhao, Z.-C. Hao, X. Shen, and T. J. Cui, "Splitting spoof surface plasmon polaritons to different directions with high efficiency in ultra-wideband frequencies," *Opt. Lett.*, vol. 44, no. 13, p. 3374, Jul. 2019, doi: 10.1364/OL.44.003374.

[18] X. Gao, J. H. Shi, X. Shen, H. F. Ma, W. X. Jiang, L. Li, and T. J. Cui, "Ultrathin dual-band surface plasmonic polariton waveguide and frequency splitter in microwave frequencies," *Appl. Phys. Lett.*, vol. 102, no. 15, Apr. 2013, Art. no. 151912, doi: 10.1063/1.4802739.

[19] B. C. Pan, P. Yu, Z. Liao, F. Zhu, and G. Q. Luo, "A compact filtering power divider based on spoof surface plasmon polaritons and substrate integrated waveguide," *IEEE Microw. Wireless Compon. Lett.*, vol. 32, no. 2, pp. 101–104, Feb. 2022, doi: 10.1109/LMWC.2021.3116169.

[20] P. H. He, D. Yao, H. C. Zhang, J. Wang, D. Bao, and T. J. Cui, "Ultra-compact on-chip spoof surface plasmon polariton transmission lines with enhanced field confinements," *J. Phys., Photon.*, vol. 4, no. 4, Oct. 2022, Art. no. 044002, doi: 10.1088/2515-7647/ac9874.

[21] P. H. He, H. C. Zhang, X. Gao, L. Y. Niu, W. X. Tang, J. Lu, L. P. Zhang, and T. J. Cui, "A novel spoof surface plasmon polariton structure to reach ultra-strong field confinements," *Opto-Electron. Adv.*, vol. 2, no. 6, pp. 19000101–19000107, 2019, doi: 10.29026/oea.2019.190001.

[22] P. H. He, L. Y. Niu, Y. Fan, H. C. Zhang, L. P. Zhang, D. Yao, W. X. Tang, and T. J. Cui, "Active odd-mode-metachannel for single-conductor systems," *Opto-Electron. Adv.*, vol. 5, no. 8, 2022, Art. no. 210119, doi: 10.29026/oea.2022.210119.

[23] Y. Liu, K.-D. Xu, Y.-J. Guo, and Q. Chen, "High-order mode application of spoof surface plasmon polaritons in bandpass filter design," *IEEE Photon. Technol. Lett.*, vol. 33, no. 7, pp. 362–365, Apr. 2021, doi: 10.1109/LPT.2021.3063522.

[24] Z. Lin, Y. Li, L. Li, Y.-T. Zhao, J. Xu, and J. Chen, "Miniaturized bandpass filter based on high-order mode of spoof surface plasmon polaritons loaded with capacitor," *IEEE Trans. Plasma Sci.*, vol. 51, no. 1, pp. 254–260, Jan. 2023, doi: 10.1109/TPS.2022.3232850.

[25] Y. Liu and K.-D. Xu, "Bandpass filters using grounded stub-loaded microstrip periodic structure for suppression of modes," *J. Phys. D, Appl. Phys.*, vol. 55, no. 42, Oct. 2022, Art. no. 425104, doi: 10.1088/1361-6463/ac8206.

[26] Z. X. Wang, H. C. Zhang, J. Lu, P. Xu, L. W. Wu, R. Y. Wu, and T. J. Cui, "Compact filters with adjustable multi-band rejections based on spoof surface plasmon polaritons," *J. Phys. D, Appl. Phys.*, vol. 52, no. 2, Jan. 2019, Art. no. 025107, doi: 10.1088/1361-6463/aae885.

[27] E. Farokhipour, M. Mehrabi, N. Komjani, and C. Ding, "A spoof surface plasmon polaritons (SSPPs) based dual-band-rejection filter with wide rejection bandwidth," *Sensors*, vol. 20, no. 24, p. 7311, Dec. 2020, doi: 10.3390/s20247311.

[28] S. Zhu, P. Wen, and Y. Liu, "Multi-band propagation of spoof surface plasmon polaritons by its high-order modes," *Jpn. J. Appl. Phys.*, vol. 61, no. 7, Jul. 2022, Art. no. 070907, doi: 10.35848/1347-4065/ac748f.

[29] S. Sun, Y. Cheng, H. Luo, F. Chen, and X. Li, "Notched-wideband bandpass filter based on spoof surface plasmon polaritons loaded with resonator structure," *Plasmonics*, vol. 18, no. 1, pp. 165–174, Feb. 2023, doi: 10.1007/s11468-022-01755-z.

[30] K.-D. Xu, S. Lu, Y.-J. Guo, and Q. Chen, "High-order mode of spoof surface plasmon polaritons and its application in bandpass filters," *IEEE Trans. Plasma Sci.*, vol. 49, no. 1, pp. 269–275, Jan. 2021, doi: 10.1109/TPS.2020.3043889.

[31] W. Li, Z. Qin, Y. Wang, L. Ye, and Y. Liu, "Spoof surface plasmonic waveguide and its band-rejection filter based on H-shaped slot units," *J. Phys. D, Appl. Phys.*, vol. 52, no. 36, Sep. 2019, Art. no. 365303, doi: 10.1088/1361-6463/ab2b28.

[32] L. Tan, Q. Wang, Y.-J. Guo, J. Cui, and K.-D. Xu, "Bandpass filter based on spoof surface plasmon polaritons with a switchable high-selectivity notch band," *Frontiers Phys.*, vol. 9, Aug. 2021, Art. no. 754510, doi: 10.3389/fphy.2021.754510.

[33] H. Zhao, P. Zhou, Z. Xu, S. Li, M. Yang, L. Liu, and X. Yin, "Tri-band band-pass filter based on multi-mode spoof surface plasmon polaritons," *IEEE Access*, vol. 8, pp. 14767–14776, 2020, doi: 10.1109/ACCESS.2020.2966257.

[34] T. Jiang, L. Shen, X. Zhang, and L. X. Ran, "High-order modes of spoof surface plasmon polaritons on periodically corrugated metal surfaces," *Prog. Electromagn. Res. M*, vol. 8, pp. 91–102, 2009, doi: 10.2528/PIERM09062901.

[35] X. Liu, Y. Feng, B. Zhu, J. Zhao, and T. Jiang, "High-order modes of spoof surface plasmonic wave transmission on thin metal film structure," *Opt. Exp.*, vol. 21, no. 25, p. 31155, Dec. 2013, doi: 10.1364/OE.21.031155.

[36] P. H. He, Y. Fan, H. C. Zhang, L. P. Zhang, M. Tang, M. Wang, L. Y. Niu, W. Tang, and T. J. Cui, "Characteristic impedance extraction of spoof surface plasmon polariton waveguides," *J. Phys. D, Appl. Phys.*, vol. 54, no. 38, Sep. 2021, Art. no. 385102, doi: 10.1088/1361-6463/ac0460.

[37] Y. Peng and W. Zhang, "Compact sub-wavelength microstrip band-reject filter based on inter-digital capacitance loaded loop resonators," *Microw. Opt. Technol. Lett.*, vol. 52, no. 1, pp. 166–169, Jan. 2010, doi: 10.1002/mop.24885.

SIYU YANG is currently pursuing the master's degree with the Chengdu University of Technology, Chengdu, China. Her current research interests include spoof surface plasmon polaritons and microwave circuits.

SHUANG LIU received the Ph.D. degree in electromagnetic field and microwave technology from the University of Electronic Science and Technology of China (UESTC), Chengdu, China, in 2016.

She is currently a Teacher with the Chengdu University of Technology, Chengdu. Her current research interests include microwave, millimeter-wave, and terahertz passive circuits, antenna, spoof surface plasmon polaritons, and physics.

FACHUN HE is currently pursuing the master's degree with the Chengdu University of Technology, Chengdu, China. His current research interests include spoof surface plasmon polaritons and microwave circuits.

HUALI ZHU received the B.S. degree from the University of Electronic Science and Technology of China, Chengdu, China, in 2017, where he is currently pursuing the Ph.D. degree in electronic science and technology.

His current research interests include microwave/millimeter wave circuit theory and technology, mm-wave, and terahertz integrated circuits and systems.

LIANGJING WANG is currently pursuing the master's degree with the Chengdu University of Technology, Chengdu, China. Her current research interests include ultrasonic detection and microwave circuits.

DAN LEI received the B.S. degree in applied physics from Chongqing University, in 2000, and the M.Eng. degree in electromagnetic field and microwave technology from the University of Electronic Science and Technology of China, in 2007.

She is currently teaching electrodynamics and microwave technology and antennas with the Chengdu University of Technology. Her current research interests include numerical modeling methods of passive microwave circuits, microwave circuits, and microwave tests.

CHAN GAO received the B.S. degree in applied physics from the Henan University of Technology, Zhengzhou, China, in 2012, and the Ph.D. degree in condensed matter physics from the University of Science and Technology of China (USTC), Hefei, China, in 2018.

From 2018 to 2021, she was a Postdoctoral Researcher with USTC. She is currently a Lecturer with the Chengdu University of Technology (CDUT), Chengdu, China. Her current research interests include the structure and photoelectrical properties of material under extreme conditions and microwave circuits.

JUN YAN received the B.S. and Ph.D. degrees in electromagnetic and microwave engineering from the University of Electronic Science and Technology of China, Chengdu, China, in 2005 and 2016, respectively.

He is currently an Engineer of microwave engineering with the China Electronics Technology Group Corporation 10th Research Institute, Chengdu. His research interests include wide-band, low-profile antenna arrays, and feed-network design for microwave and millimeter-wave frequencies.

SHUANG LIU received the Ph.D. degree in optical engineering from the Nanjing University of Science and Technology, in 2019.

She is currently a Lecturer with the Chengdu University of Technology (CDUT), Chengdu, China. Her current research interests include femtosecond laser processing and laser ultrasonic nondestructive testing.